Available online at www.sciencedirect.com
SCIENCE DIRECT®
ELSEVIER
Nuclear Physics A 753 (2005) 251–262
NUCLEAR PHYSICS A

Maximally aligned states in the proton drip line nucleus ^{106}Sb

D. Sohler [a,*], M. Palacz [b], Zs. Dombrádi [a], M. Hjorth-Jensen [c], C. Fahlander [d], L.-O. Norlin [e], J. Nyberg [g], T. Bäck [e], K. Lagergren [e,f], D. Rudolph [d], A. Algora [a], C. Andreoiu [d], G. de Angelis [h], A. Atac [i], D. Bazzacco [j], J. Cederkäll [e], B. Cederwall [e], B. Fant [k], E. Farnea [h,l], A. Gadea [h,l], M. Górska [m], H. Grawe [m], N. Hashimito-Saitoh [m], A. Johnson [e], A. Kerek [e], W. Klamra [e], J. Kownacki [b], S.M. Lenzi [h], A. Likar [n], M. Lipoglavšek [n], M. Moszyński [o], D.R. Napoli [h], C. Rossi-Alvarez [j], H.A. Roth [p], T. Saitoh [m], D. Seweryniak [q], Ö. Skeppstedt [p], J. Timár [a], M. Weiszflog [r], M. Wolińska [b]

[a] *Institute for Nuclear Research, Debrecen, Hungary*
[b] *Heavy Ion Laboratory, University of Warsaw, Warsaw, Poland*
[c] *Department of Physics and Center of Mathematics for Applications, University of Oslo, Norway*
[d] *Department of Physics, Lund University, Lund, Sweden*
[e] *Royal Institute of Technology, Stockholm, Sweden*
[f] *Department of Physics, Florida State University, Tallahassee, FL, USA*
[g] *Svedberg Laboratory, Uppsala, Sweden*
[h] *Laboratori Nazionali di Legnaro, Padova, Italy*
[i] *Department of Radiation Sciences, Uppsala University, Uppsala, Sweden*
[j] *Dipartimento di Fisica and INFN Sezione di Padova, Padova, Italy*
[k] *Department of Physics, Helsinki University, Helsinki, Finland*
[l] *University of Valencia, Valencia, Spain*
[m] *GSI, Darmstadt, Germany*
[n] *J. Stefan Institute, Ljubljana, Slovenia*
[o] *Sołtan Institute for Nuclear Studies, Świerk, Poland*
[p] *Chalmers University of Technology, Gothenburg, Sweden*
[q] *Argonne National Laboratory, Chicago, USA*
[r] *Department of Neutron Research, Uppsala University, Uppsala, Sweden*

Received 11 June 2004; received in revised form 23 February 2005; accepted 28 February 2005

Available online 19 March 2005

0375-9474/$ – see front matter
doi:10.1016/j.nuclphysa.2005.02.153

Abstract

High-spin states in ^{106}Sb have been investigated in the ^{54}Fe(^{58}Ni, $1\alpha 1p1n$) reaction by in-beam γ-spectroscopic methods using the EUROBALL detector array equipped with charged particle and neutron detectors. On the basis of measured $\gamma\gamma$-coincidence relations, angular distributions, and linear polarization ratios a significantly extended level scheme has been constructed up to spin and parity $I^{\pi} = (19^{-})$ and $E_x \sim 6.5$ MeV. The experimental results are interpreted within the framework of the $gdsh$ shell model using a realistic effective nucleon-nucleon interaction. Candidates for states with fully aligned angular momenta in the $\pi(d_{5/2}, g_{7/2})^1 \nu(d_{5/2}, g_{7/2})^5$ valence space are identified at 4338 and 5203 keV, as well as in the $\pi(d_{5/2}, g_{7/2})^1\ \nu(d_{5/2}, g_{7/2})^4 h^1_{11/2}$ space at 6087, 6573 and 6783 keV.

PACS: 23.20.Lv; 21.10.Hw; 21.60.Cs; 27.60.+j

Keywords: NUCLEAR REACTIONS ^{54}Fe(^{58}Ni, $np\alpha$), $E = 240$ MeV; measured $E\gamma$, $I\gamma$, $\gamma\gamma$-, (charged particle)γ-, (neutron)γ-coin, γ-ray polarization. ^{106}Sb deduced high-spin levels, J, π, configurations. Euroball, ISIS arrays.

1. Introduction

The structure of nuclei close to the limits of stability has become one of the central contemporary research topics in nuclear physics. Medium-heavy neutron-deficient nuclei at or beyond the proton drip line are of particular interest. While the proton drip line has been delineated between $Z \sim 28$ and $Z \sim 50$ by means of a series of fragmentation reactions [1,2], it is possible to conduct in-beam γ-ray spectroscopy of excited states in ground-state proton-emitting nuclei, such as ^{105}Sb [3,4], ^{109}I [5] or ^{113}Cs [5,6], just above the $Z = 50$ shell closure. Interestingly enough, the combination of powerful Ge detector arrays with efficient ancillary detector systems has led to the discovery of high-spin states in Ni and Cu isotopes, which decay by discrete-energy proton emission in direct competition with γ-decay [7–9]. Since neutron-deficient Sb isotopes are weakly bound with respect to the neighbouring Sn isotopes, they are also candidates for this new class of decay. A possible case is ^{106}Sb with a proton separation energy of not more than some 400 keV [10].

The nucleus ^{106}Sb was produced via a heavy-ion fusion–evaporation reaction, which allows for a search for maximally aligned states at the same time. High-spin studies in the vicinity of closed shells are well suited to discriminate excited states, which are built on configurations, where all the single-particle angular momenta of few valence nucleons are maximally aligned along one axis. Such states have already been observed in, for example, ^{98,99}Ag [11,12] or ^{98}Pd [13] and are analogous to states denoting band termination in somewhat heavier nuclei with more valence nucleons like ^{100,102,103}Pd [14–16], ^{101,102}Rh [17,18] and $^{98–100}$Ru [19]. The states in the termination region have similar single-particle

* Corresponding author. Institute of Nuclear Research, Pf. 51, H-4001 Debrecen, Hungary.
E-mail address: sohler@atomki.hu (D. Sohler).

characteristics as the maximally aligned configurations in the nuclei closer to doubly-magic ^{100}Sn.

Excited states in ^{106}Sb have previously been observed via the reaction ^{54}Fe(^{58}Ni, $1\alpha 1p1n$) and using both the NORDBALL Ge detector array [20] and a pre-EUROBALL set-up [21]. The yrast states have been known up to spin and parity $I^{\pi} = (10^{+})$ at an excitation energy of $E_x \sim 4$ MeV. In addition, an E2-decaying isomeric state with a half life of $T_{1/2} = 232(21)$ ns has been found at 103 keV in a dedicated investigation of delayed γ-rays and conversion electrons following the reaction ^{50}Cr(^{58}Ni, $1p1n$) [21]. In these studies the excited states have been interpreted with the help of rather restrictive shell-model calculations. More recently, the known experimental yrast states in ^{106}Sb have been described by large-scale shell-model calculations employing a realistic effective interaction for neutrons and protons in the single-particle valence space comprising the $2s_{1/2}$, $1d_{5/2}$, $1d_{3/2}$, $0g_{7/2}$ and $0h_{11/2}$ orbits [22].

The present paper aims at extending the experimental information in the near drip line nucleus ^{106}Sb. Section 2 presents the experimental procedure followed by an extended large-scale shell-model description in Section 3.

2. Experimental methods and results

The experiment was carried out at the tandem accelerator of Laboratori Nazionali di Legnaro in Italy. The 240 MeV beam of ^{58}Ni impinged on a 1.4 mg/cm^2 thick ^{54}Fe target enriched to 99.9% and deposited on a gold backing of 13.0 mg/cm^2. Gamma-rays were detected using the EUROBALL multi-detector array [23], comprising 26 clover [24] and 15 cluster [25] composite Compton-suppressed Ge detectors. For reaction channel identification the γ-rays were measured in coincidence with charged particles and neutrons emitted by the ^{112}Xe compound nucleus. The detection of the light charged particles was performed by means of the ISIS detector ball [26] equipped with 40 silicon ΔE–E telescopes covering $\sim 90\%$ of the total solid angle around the target. The difference in stopping powers of protons and α-particles was used to discriminate between them. The average efficiency for detection and identification of protons and α-particles was about 55% and 37%, respectively. The forward 1π solid angle was covered by the neutron wall [27] consisting of 50 liquid scintillator detectors. The neutron wall assisted in deducing the neutron multiplicity of each event. The neutron and γ-ray signals in the neutron detectors were distinguished by the pulse shape discrimination technique based on the zero-cross-over principle combined with the time-of-flight method. The logical OR of the time-aligned signals from the constant fraction discriminators of the neutron detectors was used as a common time reference for all other signals. Data were collected in an event-by-event mode. An event was recorded if either at least 1 γ-ray was detected by the Ge detectors in coincidence with one neutron in the neutron wall, or 7 γ-rays were observed in the Ge detectors. A total of about 2×10^9 events were collected during the experiment.

The ^{106}Sb nucleus was produced by the emission of one α-particle, one proton and one neutron from the compound nucleus. In the off-line data analysis a set of $\gamma\gamma$-coincidence matrices were sorted by requiring different conditions on the number of detected charged

particles and neutrons. In the $1\alpha 1p1n$ particle gated $\gamma\gamma$-coincidence matrix a strong contamination from ^{105}Sn arising from the $1\alpha 2p1n$ channel was present due to the non-detection of the second proton. The $1\alpha 1p1n$ coincidence matrix also contained γ-rays of ^{104}Sn ($1\alpha 2p2n$) and ^{104}In ($1\alpha 3p2n$), since some of the emitted particles were not detected either. However, gating on unique γ-rays from ^{106}Sb resolved the problems with these contaminations. The $\gamma\gamma$-coincidence matrices were analyzed in detail using a standard gating procedure with the help of the RADWARE software package [28]. Typical $\gamma\gamma$-coincidence spectra are presented in Fig. 1.

Energies and relative intensities of the γ transitions of ^{106}Sb determined from the $\gamma\gamma$-coincidence matrix are given in Table 1. The energy range of the γ-ray spectra was set to 4 MeV in order to observe possible higher energy transitions. The systematic errors due to the energy and efficiency calibrations were estimated to be ~ 0.3 keV and $\sim 5\%$, respectively. A total of 44 transitions were assigned to the studied nucleus, 34 of which are new. Although we could observe the 103 keV transition depopulating the isomeric state [21], a part of the intensity of this transition was lost due to the relatively long lifetime of the initial state.

Multipolarities of the γ-rays were obtained by means of a simplified $\gamma\gamma$-correlation analysis. The angular distribution ratio $R_{\text{ang}} = I_{\Theta_1}/I_{\Theta_2}$ was deduced from $1\alpha 1p1n$ particle-gated $\gamma\gamma$-coincidence matrices. For this purpose two matrices were created. In the first matrix those events were sorted where a transition was detected by the cluster detectors placed at $\sim 123^\circ$ and $\sim 164^\circ$ relative to the beam direction in coincidence with a γ-ray observed in any direction. The second matrix was created in a similar way using those $\gamma\gamma$-coincidence events where at least one of the γ rays was observed by the clover detectors at $\sim 73^\circ$ and $\sim 107^\circ$. Peak intensities I_{Θ_1} and I_{Θ_2} were determined in spectra gated by γ-rays seen in any direction. The R_{ang} ratio obtained is sensitive to the angular momentum transferred by the γ-ray. In order to reduce the uncertainty of the measured R_{ang} values we took the weighted average of several intensity ratios determined by using different coincident γ-rays as gating transitions. The dependence of R_{ang} ratios on the multipolarity of the gating transition was found normally to be smaller than the typical uncertainties in the peak fitting. Because of this neglected effect a $\Delta R_{\text{ang}} = 0.1$ systematic error was taken into account in the uncertainties given in Table 1. In this geometry the ratio R_{ang} for known stretched quadrupole transitions has an average value of $R_{\text{ang}} = 0.97$ and that of known stretched dipole transitions is $R_{\text{ang}} = 0.60$. The angular distribution ratios obtained in this way for already known transitions of ^{106}Sb are consistent with the previous assignments [20,21]. The results of the angular distribution analysis are given in Table 1.

The multipolarity assignments were further corroborated by extracting the electromagnetic characters of the transitions using the linear polarisation of the γ-rays. For this purpose, the four-element clover detectors placed close to 90° relative to the beam direction were used as Compton polarimeters [29]. Two spectra were constructed from the γ-events detected in coincidence with $1\alpha 1p1n$. The scattered γ-rays were added back, and the scattering events taking place perpendicular and parallel to the reaction plane were

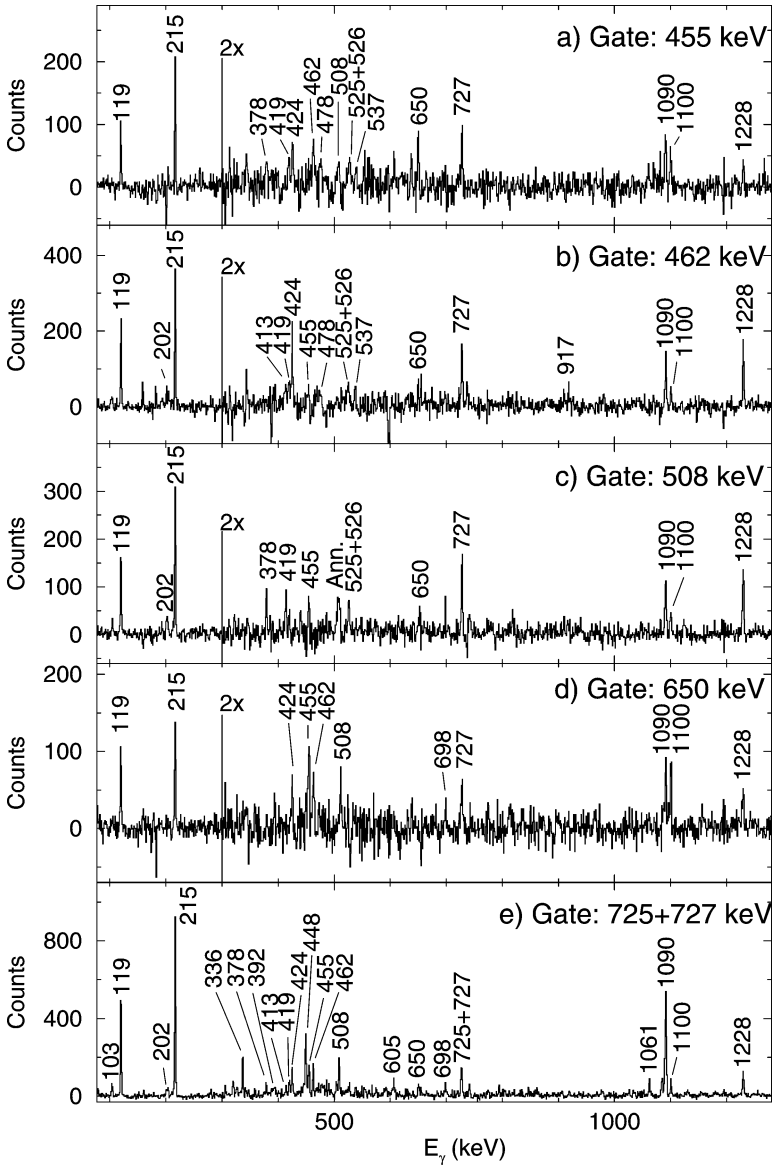

Fig. 1. Typical $\gamma\gamma$-coincidence spectra of ^{106}Sb.

collected in the first and second spectra, respectively. Assuming that each clover crystal has equal efficiency, an experimental linear polarisation is defined as

$$P = \frac{1}{Q}\frac{N_\perp - N_\parallel}{N_\perp + N_\parallel}, \tag{1}$$

Table 1
Energies, relative intensities, angular distribution ratios, linear polarisations, and deduced multipolarities of the transitions from the ^{54}Fe(^{58}Ni, $1\alpha 1p1n$)^{106}Sb reaction

E_γ (keV)	I_γ (rel.)	R_{ang}	P	Mult.	E_i (keV)	$I_i^\pi \rightarrow I_f^\pi$
103.4(3)	12.0(9)				103	$(4^+) \rightarrow (2^+)$
118.8(3)	91.0(50)	0.58(11)		D	437	$(6^+) \rightarrow (5^+)$
202.2(3)	10.8(8)	0.59(11)	−0.7(5)	M1	2254	$(10^+) \rightarrow (9^+)$
215.4(3)	100.0(60)	0.63(11)	−0.5(2)	M1	318	$(5^+) \rightarrow (4^+)$
281.2(3)	2.0(3)				3763	$(13^+) \rightarrow (12^+)$
319.0(3)	2.6(4)	0.59(11)		D	6087	$(18) \rightarrow (17^-)$
326.1(3)	1.5(3)				2491	$(10^+) \rightarrow (9^+)$
335.7(3)	4.4(5)				3315	
377.6(3)	4.0(4)	0.66(12)		(D)	4368	$(14^-) \rightarrow (13^-)$
392.4(3)	4.5(7)				1527	$(8^+) \rightarrow (7^+)$
413.4(4)	8.2(7)	1.03(14)	0.6(4)	E2	2254	$(10^+) \rightarrow (8^+)$
419.0(3)	5.2(5)	0.59(11)	−0.6(5)	M1	5768	$(17^-) \rightarrow (16^-)$
424.3(4)	11.5(10)	0.65(11)	−0.5(3)	M1	4368	$(14^-) \rightarrow (13^-)$
448.0(4)	19.1(14)	0.62(11)	−0.9(4)	M1	2702	$(11^+) \rightarrow (10^+)$
455.0(4)	15.9(12)	0.59(11)	−0.3(3)	M1	4823	$(15^-) \rightarrow (14^-)$
461.6(4)	8.4(7)	0.66(11)	0.9(5)	E1	3944	$(13^-) \rightarrow (12^+)$
478.2(3)	2.4(6)				6783	$\rightarrow (18)$
508.4(3)	7.1(7)	0.64(11)	0.8(5)	E1	3990	$(13^-) \rightarrow (12^+)$
524.6(3)	3.1(7)				2052	$(9^+) \rightarrow (8^+)$
526.0(3)	5.2(5)	0.55(11)	−0.7(8)	M1	5349	$(16^-) \rightarrow (15^-)$
537.0(3)	2.6(3)	0.61(11)		D	6305	$(18) \rightarrow (17^-)$
559.7(4)	5.2(6)	1.04(14)		Q	3944	$(13^-) \rightarrow (11^-)$
574.8(4)	2.8(3)				4338	$(13, 14^+) \rightarrow (13^+)$
604.6(4)	5.4(5)	0.55(11)		D	4368	$(14^-) \rightarrow (13^+)$
637.9(4)	14.2(12)	0.65(11)	−0.1(2)	M1	2165	$(9^+) \rightarrow (8^+)$
649.7(3)	8.7(7)	1.04(12)		Q	6573	$(19^-) \rightarrow (17^-)$
698.0(4)	15.7(15)	0.60(11)	−0.9(4)	M1	1135	$(7^+) \rightarrow (6^+)$
725.0(3)	6.2(8)				2979	$\rightarrow (10^+)$
726.8(4)	42.2(28)	1.08(12)	0.4(2)	E2	2254	$(10^+) \rightarrow (8^+)$
779.8(4)	2.1(5)				3482	$(12^+) \rightarrow (11^+)$
816.8(3)	8.9(8)	1.03(12)		Q	1135	$(7^+) \rightarrow (5^+)$
830.6(3)	3.5(4)				3947	$\rightarrow (11^+)$
856.0(3)	2.6(5)				4338	$(13, 14^+) \rightarrow (12^+)$
865.0(5)	2.5(4)				5203	$\rightarrow (13, 14^+)$
892.6(3)	3.1(4)	0.57(12)		D	3384	$(11^-) \rightarrow (10^+)$
917.3(4)	15.7(14)	1.02(14)	0.8(6)	E2	2052	$(9^+) \rightarrow (7^+)$
951.1(4)	8.9(9)	0.96(12)		Q	3116	$(11^+) \rightarrow (9^+)$
964.0(4)	5.6(8)	1.07(14)	0.9(10)	E2	2491	$(10^+) \rightarrow (8^+)$
1061.0(4)	8.7(10)	0.95(12)	1.5(11)	E2	3763	$(13^+) \rightarrow (11^+)$
1090.4(4)	63.4(43)	1.03(14)	0.8(3)	E2	1527	$(8^+) \rightarrow (6^+)$
1100.0(3)	10.5(9)	1.03(14)		Q	5923	$(17^-) \rightarrow (15^-)$
1129.6(3)	4.2(5)				3384	$(11^-) \rightarrow (10^+)$
1227.88(4)	20.3(14)	0.97(12)	1.5(11)	E2	3482	$(12^+) \rightarrow (10^+)$
1404.1(4)	10.1(9)	1.22(14)	1.4(12)	E2	1841	$(8^+) \rightarrow (6^+)$

where Q is the polarisation sensitivity for the clover detectors, which is a function of the γ-ray energy [29]. $N_\perp$ and $N_\parallel$ denote the number of events scattered perpendicular and parallel to the reaction plane, respectively. $P > 0$ is characteristic for stretched E1, E2 and non-stretched M1 transitions, while $P < 0$ characterizes stretched M1 and non-stretched E1 transitions. The results of the linear polarisation analysis are also summarized in Table 1.

During the multipolarity assignments only dipole and electric quadrupole transitions were considered. In addition, it was assumed that in the heavy-ion induced fusion–evaporation reactions, high-spin states are preferably populated and their decays proceed mainly via stretched transitions along the yrast line. Thus, the maximum possible spin value allowed by the angular distribution ratios of the transitions was assigned to the states. Parity was proposed to a state if E1, M1 or quadrupole character could be determined for one of the transitions connecting it to a state with known parity. The electric quadrupole multipolarity of the 103 keV transition was adopted from Ref. [21] where this assignment was determined from delayed γ-ray and conversion electron measurements. The multipolarities obtained are listed in Table 1, along with the deduced spins and parities of the initial and final states.

The proposed level scheme shown in Fig. 2 was constructed on the basis of $\gamma\gamma$-coincidence relations, energy and intensity balances. The order of the transitions in the γ-ray cascades was deduced from the intensity relations. This level scheme is basically consistent with the previous results [20,21], except for some minor differences. Furthermore, we could observe several new excited states due to the higher efficiency of the used detector set-up. In the main sequence the previous placement of the lowest-lying 103, 215, 119, 1090 and 727 keV γ-rays [21] are in agreement with our $\gamma\gamma$-coincidence data. They are continued by the 1228 and 856 keV transitions establishing states at 3482 and 4338 keV. The cascade of γ-rays with energies of 455, 526, 419, 537 and 478 keV is connected to the main branch at 3482 keV via the 462–424 and 508–378 keV transitions. In this way the order of the 1228 and the 508 keV transitions is reversed compared to Ref. [21]. This change is supported by the spectrum gated on the 462 keV γ-ray shown in Fig. 1(b), where it can be seen that it is in coincidence with the 1228 keV transition but not with the 508 keV one. The parallel placement of the 462–424 and 508–378-keV γ-ray cascades is based on the coincidence spectra gated by γ-rays lying either below or above them like those shown in Fig. 1(a) and (e). In the spectra obtained by gating on the members of these two pairs their partner γ-lines are visible, but the members of the other pair are not. For instance, the 424 keV γ-ray appears in the gate spectrum of the 462 keV transition shown in Fig. 1(b), but the 378 and 508-keV peaks are missing. Vice versa, the 378 keV transition is present in the spectrum gated on the 508 keV transition in Fig. 1(c), but the 424 and the 462 keV γ-rays are not. In the gate spectrum of the 508 keV γ-ray a broader peak appears at about 510 keV. Decreasing the width and shifting the position of the gating γ-line the height of this peak changes faster than those of other γ-lines in coincidence with the 508 keV transition. Thus, we assign this wider peak to the 511-keV annihilation γ-ray, although it has to be mentioned that it does not disappear completely even with a careful gating procedure.

The corresponding coincidence relations for the continuation above the parallel sequences are presented in the spectra gated by the 455, the 462 and the 508-keV transitions

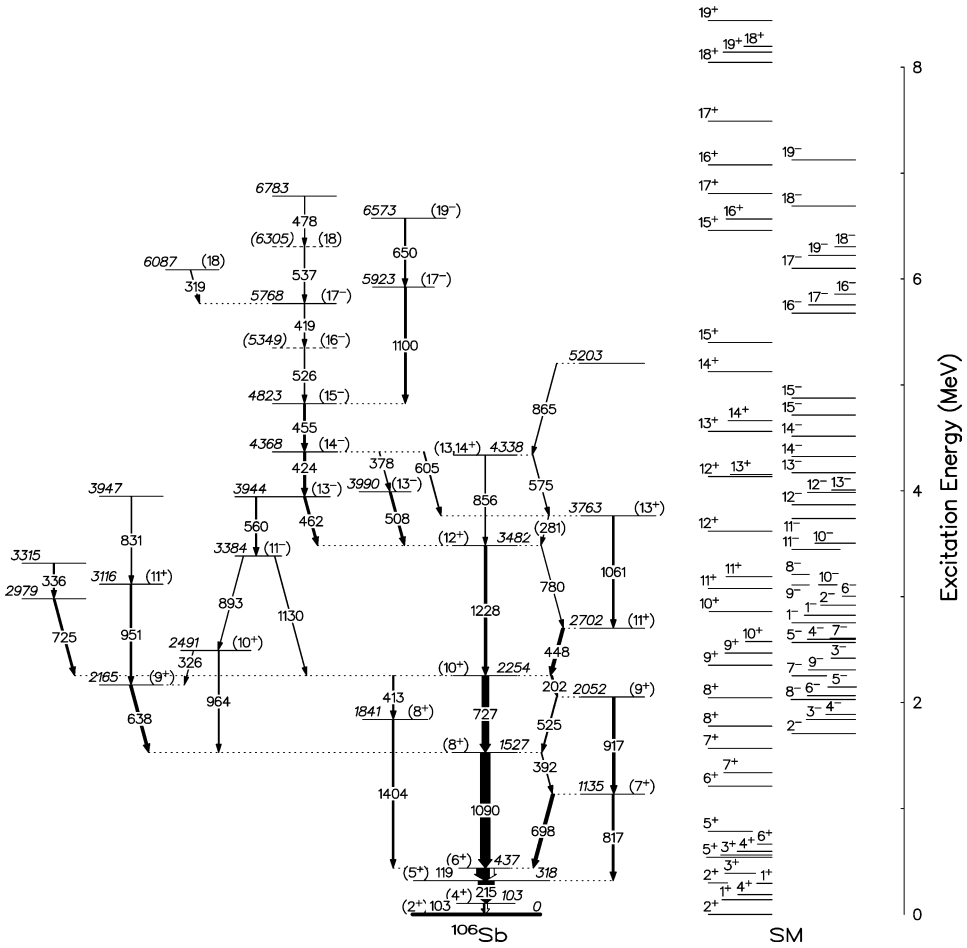

Fig. 2. Proposed experimental level scheme of ^{106}Sb in comparison with results of shell model calculations. First two lowest-lying calculated states for each spin and parity are shown.

in Fig. 1(a), (b) and (c). The levels at 5349 and 6305 keV remain ambiguous due to the uncertain order of the 526 and the 419, as well as the 537 and the 478 keV transitions.

The level of 4823 keV in the above mentioned cascade is populated by another branch consisting of the 1100 and the 650 keV γ-rays, establishing the levels at 5923 and 6573 keV excitation energies. Their placement is supported by the spectrum gated on the 650 keV γ-ray presented in Fig. 1(d). In this spectrum the intensities of the 727, 1090, 455 and 1100 keV γ-lines are similar, which strengthens the assumption that the 650 keV transition is placed above the 1100 keV one. Nevertheless, the 1228, 462 and 424 keV γ-lines seem to be weaker as it is expected from the level scheme, similarly to the spectrum gated on the 455 keV γ-ray. Taking the gate spectra of the 462 and the 508 keV transitions which connect the 650 and the 455 keV γ-rays to the lower-lying part, the intensity of the 1228 keV γ-line becomes again as strong as those of the 727 and 1090 keV transitions

continuing the main sequence to the ground state. This may indicate the existence of other, non-observed weak branches between the levels at 4823 and 2254 keV.

A side branch containing the 698, 392, 525, 202, 448, 780, 281, 575 and 865 keV γ-rays is linked to the main sequence and is built up to 5203 keV excitation energy. Some of the cross-over transitions in this sequence with energies of 817, 917 and 1061 keV could also be observed. In Ref. [21] the cascade formed by the 448 and the 1061 keV γ-rays was connected to the third excited level at 437 keV. In the present work they are placed at a higher energy populating the level at 2254 keV as a part of the side branch. The gate spectrum of the 727 keV transition in Fig. 1(e) demonstrates the relevant coincidence relations for the new placement. In addition, the levels at 2254 and 437 keV are connected also through the 413 and 1404 keV γ-rays establishing the state at 1841 keV.

From the state at 3944 keV an additional γ-ray sequence decays to the low-lying part of the level scheme connecting the levels at 2491 and 3384 keV. Furthermore, side feedings of the states at 1527 and 2254 keV come via the γ-ray cascades with energies of 831–951–638 keV and 336–725 keV establishing the levels at 3947, 3315, 3116, 2979 and 2165 keV.

For the ground state in ^{106}Sb a tentative spin-parity $I^\pi = (2^+)$ has been suggested from shell model calculations in Ref. [21] taking also into account the consequences of its 0.6 ± 0.2 s life time [30]. As no new experimental information is available, we adopt this tentative assignment keeping all our spin and parity values relative to it. However, it should be noted that in Ref. [21] it was not excluded that the ground state could have spin and parity $I^\pi = 1^+$ either. This would lower all spin values by one unit.

We also adopt the $I^\pi = (4^+)$ value for the isomeric state at 103 keV proposed in Ref. [21]. Above this state the previously made spin and parity assignments of the levels at 318, 437, 1527 and 2254 keV are confirmed by our deduced multipolarities. For the γ-rays in the ground state cascade up to the $I^\pi = (10^+)$ state parity-conserving characteristics could be determined for all but the 119 keV transition which depopulates the state at 437 keV. However, this state is connected by an M1 γ-ray to the level at 1135 keV having positive parity because of the quadrupole character of the 817 keV transition. Thus, we assign positive parity also to third excited state at 437 keV. Higher up, $I^\pi = (12^+)$ spin and parity assignment is deduced for the state at 3482 keV on the basis of the E2 multipolarity of the 1228 keV γ-ray. Besides the already known most intense transitions the $I^\pi = (10^+)$ 2254 keV level decays to the $I^\pi = (6^+)$ 437 keV state via the 1404 and 413 keV E2 γ-rays. Thus $I^\pi = (8^+)$ spin and parity is proposed for the level at 1841 keV. Parallel to this sequence the states at 2254 and 437 keV are connected by the 698 keV M1, the 917 keV E2 and the 202 keV M1 transitions as well. Therefore, we assign $I^\pi = (7^+)$ and (9^+) spins and parities to the middle-lying states at 1135 and 2052 keV. Since above them this side structure is continued by the 448 keV M1 and the 1061 keV E2 transitions, we suggest $I^\pi = (11^+)$ and (13^+) for the states at 2702 and 3763 keV. Based on yrast arguments we propose $I^\pi = (13, 14^+)$ for the 4338 keV level, which is connected to $I^\pi = (12^+)$ and (13^+) states by the 575 and 856 keV γ-rays, although multipolarities could not be deduced for them.

Above the 3482 keV level the positive parity is changed to negative parity by the 462 and the 508 keV E1 transitions indicating spin and parity $I^\pi = (13^-)$ for the states at 3944 and 3990 keV. A set of negative-parity states is then built up through M1 transitions which leads to the spin and parity assignments $I^\pi = (14^-)$, (15^-), (16^-) and (17^-) to the levels

at 4368, 4823, 5349 and 5768 keV. Since at the top of the M1 sequence dipole character is determined for the 319 and the 537 keV γ-rays feeding the $I^\pi = (17^-)$ level from the 6087 and the 6305 keV states, we assign $I = (18)$ spin value to them. Another cascade connected to the negative parity structure at the $I^\pi = (15^-)$ 4823 keV state consists of quadrupole transitions, and thus spins and parities $I^\pi = (17^-)$ and (19^-) are proposed for the levels at 5923 and 6573 keV.

The lower-lying positive-parity states are linked to the $I^\pi = (13^-)$ level at 3944 keV, besides via the strongest γ-rays, also through the 964 keV E2, the 893 keV dipole and the 560 keV quadrupole transitions. These multipolarities provide $I^\pi = (10^+)$ and (11) assignments for the states at 2491 and 3384 keV. Since the $I = (11)$ 3384 keV state is fed directly from the $I^\pi = (13^-)$ 3944 keV level by a quadrupole transition, we propose negative parity also for the former one. Concerning the group of states decaying into the $I^\pi = (8^+)$ 1527 keV state via the 638 keV M1 and the 951 keV quadrupole transitions, we suggest $I^\pi = (9^+)$ and (11^+) spins and parities for the levels at 2165 and 3116 keV based on the above multipolarities of the deexciting γ-rays. Due to the lack of statistics we could not make spin and parity assignments to the states at 2979, 3315, 3947, 5203 and 6783 keV.

3. Discussion

In the vicinity of the doubly-magic ^{100}Sn the shell model approach provides an appropriate tool to describe the experimental data including the structure of the high-spin excited states of nuclei [3]. Thus, to interpret the present experimental data the previous shell model calculations of Ref. [22] have been extended to cover the spin and energy regime reached in the present study. In the calculations ^{100}Sn is considered as an inert core. Five valence neutrons and one valence proton are placed in the single-particle orbits $2s_{1/2}$, $1d_{5/2}$, $1d_{3/2}$, $0g_{7/2}$, and $0h_{11/2}$. A realistic effective interaction based on the CD-Bonn nucleon–nucleon interaction [31] is used. More details about the effective charges and the single-particle energies used in the calculations can be found in Ref. [22]. The results of calculations are presented on the right-hand side of Fig. 2 in comparison with the experimental level scheme.

The calculations favor an $I^\pi = 2^+$ assignment for the ground state, although the first excited state with spin 1^+ lies at ~ 140 keV. In the 2_1^+ ground state the valence proton occupies mainly the $d_{5/2}$ orbit and one valence neutron resides partly in the $d_{5/2}$ orbit and partly in the $d_{3/2}$ orbit. The two neutron pairs, each coupled to I=0, are distributed among the $d_{5/2}$ and the $g_{7/2}$ orbits. This is the case also for the 4_1^+ and 5_1^+ states, while in the 6_1^+ state the odd neutron is pushed up to the $g_{7/2}$ orbit. The 7_1^+ state is the lowest-lying of the observed states where also the odd proton occupies almost exclusively the $g_{7/2}$ orbit. Since 7 is the maximum spin for the $\pi(d_{5/2}, g_{7/2})^1\nu(d_{5/2}, g_{7/2})^1$ configuration, the wave functions of all the yrast and the yrare states up to 12_1^+ include two additional neutrons distributed on the $d_{5/2}$ or the $g_{7/2}$ orbits, while the other neutron pair remains coupled to $I = 0$. From the 12_2^+ state on also the second neutron pair breaks up and all the valence neutrons contribute to the spin. Combining one proton and five neutrons in the $s_{1/2}$, $d_{5/2}$,

$d_{3/2}$ and $g_{7/2}$ orbits the maximum available spin value is 15, but allowing one more valence nucleon in the $d_{5/2}$ orbit, one can also construct fully aligned states with spin 14.

All the yrast states predicted from spin 4^+ up to 13^+ were found experimentally and also the first yrare states in the 8^+–12^+ spin region were identified. The 4338 keV state is a candidate for the fully aligned 14^+ state with a $\pi g^1_{7/2}\nu d^3_{5/2}g^2_{7/2}$ configuration, while the 5203 keV state can be assigned to the maximally aligned 14^+ state with a $\pi d^1_{5/2}\nu d^2_{5/2}g^3_{7/2}$ configuration or to the maximally aligned 15^+ state with a $\pi g^1_{7/2}\nu d^2_{5/2}g^3_{7/2}$ configuration.

Negative parity states in ^{106}Sb may arise from configurations obtained by exciting a single neutron to the $h_{11/2}$ orbit. By coupling a $h_{11/2}$ neutron and the $(d_{5/2}, g_{7/2})$ proton, negative parity states with the maximum spin 8^- and 9^- can be constructed. From spin 10, a coupling to a broken neutron pair occupying the $d_{5/2}$ and the $g_{7/2}$ orbits is also required. Above the 15^-_1 state the configurations include two broken neutron pairs in the $d_{5/2}$ and the $g_{7/2}$ orbits. In this valence space states with spin 18 and 19 can be created aligning all the spins of the $(d_{5/2}, g_{7/2})$ proton and the $h_{11/2}$ neutron, as well as of the other four valence neutrons in the mixed $(d_{5/2}, g_{7/2})$ orbit.

In the experiment negative parity yrast states and some of the yrare states in the 13–19 spin region were found. The state at 6087 keV may be interpreted as the 18^-_1 state built upon the fully aligned $\pi d^1_{5/2}\nu h^1_{11/2}d^2_{5/2}g^2_{7/2}$ configuration. The states at 6573 and 6783 keV can be candidates for the fully aligned $\pi g^1_{7/2}\nu h^1_{11/2}d^2_{5/2}g^2_{7/2}$ and $\pi g^1_{7/2}\nu h^1_{11/2}d^1_{5/2}g^3_{7/2}$ configurations, respectively. At higher spins the calculations predict negative parity states with the odd proton in the $h_{11/2}$ orbit coupled to the $h^2_{11/2}(d_{5/2}, g_{7/2})^3$ neutron configurations. The negative parity band seems to have a smoother transition between one and two broken pair configurations, which may be a sign for core polarization of the high spin $\nu h_{11/2}$ orbit making the band more collective than calculated.

As the proton separation energy in ^{106}Sb is about 400 keV, the states lying above this excitation energy might decay by emitting a proton in competition with the decays via γ-ray cascades. In such a case the lower-lying transitions of the daughter nucleus ^{105}Sn should have been observed in coincidence with some of the most probable higher-lying γ-rays of ^{106}Sb. We could not confirm the existence of such coincidence relations in the experimental data. In spite of the low proton binding energy, the protons are kept inside the nucleus by the Coulomb and centrifugal barriers. To observe a proton decay from one of the excited states in ^{106}Sb the proton has to penetrate at least the top of the Coulomb plus centrifugal barrier with a non-vanishing spectroscopic factor with $\ell = 0$, 2, 4 or 5 in the proton model space. The proton decay could compete with the γ-decay if only there is an yrast trap. In agreement with the experimental findings, the shell model calculations do not predict such a state.

4. Summary

The present work has been devoted to study the structure of the next to proton drip line nucleus ^{106}Sb produced in the ^{54}Fe(^{58}Ni, $1\alpha 1p 1n$) reaction. A positive and a negative parity $\Delta I = 1$ band-like structure has been observed with some side-feeding transitions. As a result, the system of high-spin states have been extended up to 6.8 MeV excitation energy and to spin and parity values of $I^\pi = (13, 14^+)$ and (19^-). The ex-

perimental results have been interpreted in the framework of the shell model using a realistic effective nucleon–nucleon interaction. The calculations reproduced reasonably well the observed excited states. Maximally spin aligned $\pi(d_{5/2}, g_{7/2})^1 \nu(d_{5/2}, g_{7/2})^5$ and $\pi(d_{5/2}, g_{7/2})^1 \nu(d_{5/2}, g_{7/2})^4 h^1_{11/2}$ configurations were assigned to the states at 4338, 5203 keV and at 6087, 6573, 6783 keV, respectively.

Acknowledgements

This work was supported by the Hungarian Fund for Science Research (OTKA contract No. T038404 and T046901), the Swedish Research Council, the European Commission (EC) TMR/LSF Contracts no. ERBFMGECT980110, ERBFMBICT983126, and ERBCH-BGCT940713, the Polish Scientific Research Committee grant No. 5P03B 046 20, the Bolyai János and the Göran Gustafsson Foundations, as well as the Swedish Institute within the framework of the New Visby Programme.

References

[1] M. Hencheck, et al., Phys. Rev. C 50 (1994) 2219.
[2] A. Stolz, et al., Phys. Rev. C 65 (2002) 064603.
[3] M. Lipoglavsek, et al., Phys. Rev. C 65 (2002) 051307(R).
[4] R.J. Tighe, et al., Phys. Rev. C 49 (1994) 2871(R).
[5] T. Faestermann, et al., Phys. Lett. B 137 (1984) 23.
[6] C.J. Gross, et al., in: AIP Conf. Proc., vol. 455, American Institute of Physics, Woodbury, NY, 1998, p. 444.
[7] D. Rudolph, et al., Phys. Rev. Lett. 80 (1998) 3018.
[8] D. Rudolph, et al., Phys. Rev. Lett. 82 (1999) 3763.
[9] D. Rudolph, et al., Phys. Rev. Lett. 89 (2002) 022501.
[10] G. Audi, A.H. Wapstra, C. Thibault, Nucl. Phys. A 729 (2003) 337.
[11] J. Cederkäll, et al., Eur. Phys. J. A 1 (1998) 7.
[12] D. Sohler, et al., Eur. Phys. J. A 16 (2003) 171.
[13] J. Cederkäll, et al., Z. Phys. A 359 (1997) 227.
[14] G.E. Perez, et al., Nucl. Phys. A 686 (2001) 41.
[15] J. Gizon, et al., Phys. Lett. B 410 (1997) 95.
[16] B.M. Nyakó, et al., Phys. Rev. C 60 (1999) 024307.
[17] J. Timár, et al., Eur. Phys. J. A 4 (1999) 11.
[18] J. Gizon, et al., Nucl. Phys. A 658 (1999) 97.
[19] J. Timár, et al., Phys. Rev. C 62 (2000) 044317.
[20] D. Seweryniak, et al., Phys. Lett. B 321 (1994) 323.
[21] D. Sohler, et al., Phys. Rev. C 59 (1999) 1324.
[22] T. Engeland, et al., Phys. Rev. C 61 (2000) 021302(R).
[23] J. Gerl, R.M. Lieder (Eds.), EUROBALL III, A Europian γ-Ray Facility, GSI, 1992.
[24] G. Duchêne, et al., Nucl. Instrum. Methods A 32 (1999) 90.
[25] J. Eberth, et al., Nucl. Instrum. Methods A 369 (1996) 135.
[26] E. Farnea, et al., Nucl. Instrum. Methods A 400 (1997) 87.
[27] Ö. Skeppstedt, et al., Nucl. Instrum. Methods A 421 (1999) 531.
[28] D. Radford, Nucl. Instrum. Methods A 361 (1995) 297;
D. Radford, Nucl. Instrum. Methods A 361 (1995) 306.
[29] P.M. Jones, et al., Nucl. Instrum. Methods A 362 (1995) 556.
[30] M. Lewitowicz, in: M. de Saint-Simon, O. Sorlin (Eds.), Proc. of Int. Conf. on Exotic Nuclei and Atomic Masses (ENAM 95), Edition Frontieres, Gif-sur-Yvette, 1995, p. 427.
[31] R. Machleidt, F. Sammarruca, Y. Song, Phys. Rev. C 53 (1996) R1483.